Pressure- induced structural transition and huge enhancement of superconducting properties of single-crystal $Fe_{0.99}Ni_{0.01}Se_{0.5}Te_{0.5}$ unconventional superconductor

Kalaiselvan Ganesan [1,2*], Govindaraj Lingannan[1], Kannan Murugesan[1], Christopher S. Perreault[2], Gopi K. Samudrala[2], Pankaj Kumar Maheshwari[3], V. P. S. Awana[3] and Yogesh K. Vohra[2], S. Arumugam[1*]

[1]*Centre for High Pressure Research, School of Physics, Bharathidasan University, Tiruchirappalli, 620024, India*
[2]*Department of Physics, University of Alabama at Birmingham, Birmingham, AL 35294, USA*
[3]*National Physical Laboratory (CSIR), Dr. K. S. Krishnan Road, New Delhi 110012, India*

*** Corresponding Authors:**
a. Prof. S. Arumugam, Email: - sarumugam1963@yahoo.com
Telephone no: - (O): 91-431- 2407118 Cell: 91-95009 10310;
b. Dr. G. Kalaiselvan, Email: kalai71309@gmail.com, Telephone no: - (O): +91-8610767536

Address all correspondence to these authors: email: sarumugam1963@yahoo.com

Abstract

We report high pressure structural studies (52 GPa) at room temperature combined with magnetic [(*M(T)*:1GPa] and electrical resistivity [(*ρ(T)*:0-21GPa)] measurements down to 2K on $Fe_{0.99}Ni_{0.01}Se_{0.5}Te_{0.5}$ superconductor using designer diamond anvils (D-DAC) pressure cell. The *M(T)* data shows huge enhancement of superconducting transition temperature (T_c) from 8.62 to 14.8 K (1 GPa) and *ρ(T)* reveals maximum enhancement of T_c ~ 30.5 K at 3 GPa (dT_c/dP= ~ 7.19 K/GPa) followed by moderate decrease of T_c up to 19 K at 7.5 GPa, further increasing pressure T_c gets vanished at 10.6 GPa. The reduction of T_c due to the occurrence of structural transition that is likely associated with possible reduction of charge carriers in the density of states in Fermi surface. The high pressure XRD measurements shows tetragonal phase exists up to 7 GPa, followed by mixed-phase which is visible between 7.5 GPa to 14.5 GPa. The structural transformation occurs at 15 GPa from tetragonal ($P4/nmm$) to NiAs -type hexagonal phase

(*P6$_3$/mmc*) and it is stable up to 52 GPa were confirmed from the equation of state (EOS) and it can be correlated with variation of T_c under pressure for $Fe_{0.99}Ni_{0.01}Se_{0.5}Te_{0.5}$ chalcogenide superconductors.

Keywords: Fe-chalcogenide, High T_c-Superconductors, Structural studies, Phase transformation,

Introduction

The discovery of high-temperature superconductivity in iron-chalcogenides (FeSe) [1], exhibits a PbO type tetrahedral crystal lattice, which is generated much scientific attention due to its simplest crystal structure among various other Fe-based superconductors [2]. The superconducting phenomenon of this layers FeSe compound exhibiting edge-sharing $FeSe_4$ tetrahedron has created remarkable attention in the effects of internal (chemical) and external pressure on these 11 type systems [3-5]. The ion substitution is a convenient technique for creating efficient internal pressure, which has been widely used in the iron and cuprate based superconductors [6,7]. On the other hand, the highest superconducting transition temperature (T_c) is observed at 9 K in Se deficient FeSe [8-9] and the partial substitutions of Te in the Se site $[Fe(Se_{1-x}Te_x)_{0.82}]$ gives a large increment of T_c up to ~ 14 K [10]. Further, the chemical pressure generated by the doping with similar valance and different atomic radius elements such as S, Se and Te in $FeSe_{1-x}Te_x$ [10-11]. Among the various possible substitutions, the partial replacement of transition-metal (Tm) ion substitution such as Ni ~ 8.7 K [12-14], Co ~ 11 K [15,16], Mn~ 5 K [17] at the Fe site in $Fe_{1-x}Tm_xSe_{0.5}Te_{0.5}$ compound gives answers for most informative queries such as the pairing symmetry and the low-energy excitations. Moreover, a huge enhancement of T_c up to 37 K at 8.9 GPa with pressure coefficient of 9.1 K/GPa has been reported in FeSe layered material [3]. However, the effect of chemical and external pressure is not comparable in enhancing the superconducting properties of the undoped FeSe system.

The external pressure is one of the major tools to study the superconducting properties more efficiently and changing the following parameters such as the bond lengths, bond angles and lattice constants, which may vary the charge carrier in the density of states at the Fermi surface. In 2009, Horigane *et al*., correlated structural distortion with their change in T_c of Te doped α-FeSe compounds [18, 19] and such study gives a stimulated interest to focus on the detailed investigations on both electronic and structural properties of these materials under very high pressures and low temperatures. Furthermore, numerous high-pressure studies have been reported on optimally Te-doped FeSe system ($FeSe_{0.55}Te_{0.45}$), and the T_c is found to enhance sharply up to 23 K at 2.3 GPa, further, an increase of pressure leads to decrease of T_c in the monoclinic phase and get completely suppressed at 11.9 GPa [20–23]. Further application of pressure in this material (11.9 GPa to 15 GPa) $\rho(T)$ exhibits a metallic behaviour up to 15 GPa. Gresty *et al*., and Stemshorn *et al*., reported two new observations under pressure in the same compound, namely, a distorted monoclinic (above 3 GPa) and amorphization (above 11.5 GPa) [20,24]. However, various theoretical and experimental investigations exhibit the change in magnetic ordering, superconducting, and electronic properties which might be depending on the variation of chalcogen height in $FeSe_{1-x}Te_x$ compounds [25–27]. Further, tetragonal to orthorhombic structural phase transition occurs at 90 K [28], and superconductivity emerged at 9.3 K without long-range magnetic ordering has been reported in $Fe_{1.01}Se$ [28-29]. The powder XRD measurements on undoped FeSe under high pressure gives detailed structural information to understand the variation of superconducting T_c of this system. Further, it is found that both Fe-Se-Fe bond angle (α) decreased from 104.53˚ to 103.2˚ and T_c significantly increases to 37 K with the application of pressure up to 9 GPa, while $FeSe_4$ tetrahedron changes from the regular tetrahedron to disorder one [3,4]. On the other hand, FeSe exhibits the rapid increase of T_c up to

2 GPa due to a decrease of anion height with the application of pressure. Further, enhancing pressure, the anion height reaches a minimum value of 1.42 Å at 6 GPa. Above 6 GPa, an increase of anion height has been correlated with the decrease of T_c. Furthermore, T_c got suppressed at higher pressures 10.2 GPa where the structural phase transition occurs from tetragonal to hexagonal phase [30,31]. Therefore, the detailed experimental investigation on the structural, magnetic, and transport properties under high pressure helps to understand the electronic and structural changes of this compound. This correlated effect expected to help us for understanding the behaviour of pressure effect on T_c and also to make a comparison with the transition-metal doped $Fe_xTm_{1-x}Se_{0.5}Te_{0.5}$ samples.

To our knowledge, this is a first report on detailed studies of the structural evolution of $Fe_{0.99}Ni_{0.01}Se_{0.5}Te_{0.5}$ single crystalline material under pressure (52 GPa) using Diamond Anvil Cell (DAC) and synchrotron source at RT. Also, the electrical resistivity measurements under pressure have been performed using both piston-cylinder pressure cell up to ~3 GPa (down to 2 K) and Designer-Diamond Anvil Cell (D-DAC~21 GPa) down to 12 K. The tetragonal *P4/nmm* structure starts change to $P6_3/mmc$ -NiAs hexagonal phase at ~15 GPa. These results are discussed and correlated with the pressure dependence of T_c, normal state resistivity $\rho(T)$ and magnetic [$M(T)$ & $M(H)$] measurements.

Results and discussions

Structural Properties

Figure 1(a) shows the X-ray diffraction spectra of $Fe_{0.99}Ni_{0.01}Se_{0.5}Te_{0.5}$ at RT with an initial pressure of 0.5 GPa and it shows a phase pure sample, and there is no detectable contamination of any impurity phases. It shows a tetragonal structure (space group *P4/nmm*) with lattice parameters: a= 3.79075 Å, c= 6.02839 Å, and the calculated volume (V_0): 86.627 $Å^3$,

which are very close to the value, reported by Maheshwari *et al*., [14] at ambient pressure. The diffraction patterns remain almost unchanged with the application of pressure up to 7 GPa, and above which the intensity of diffraction peaks reduces. Further, some additional peaks have also appeared simultaneously at the shoulder of the major diffraction peaks which indicates a structural transition begins from tetragonal to hexagonal phase at 7.5 GPa as shown in Figure 1(b). While increasing the application of pressure, the observed additional peaks are very well indexed with the NiAs – hexagonal (*P6$_3$/mmc*) structure [20] and it starts appearing more and found that both tetragonal and hexagonal phases co-exist between 7.5 –14 GPa. Further, the application of pressure, structural phase transition occurs from tetragonal to NiAs-hexagonal (*P6$_3$/mmc*) type at 15 GPa and the lattice parameters a= 3.727 Å, c=5.168 Å, and volume (V_0) 63.39 Å^3 are shown in Figure. 1(c). The hexagonal structure remains unchanged with an increase of pressure from 15 GPa to 52 GPa [Figure. 1(d)] and it is the highest pressure attained in our experiment and lattice parameters are found to be a= 3.490 Å, c= 5.021 Å, and V=52.97 Å^3, as shown in Figure. 1(d). The structural transition observed at 15 GPa is reversible while the pressure is released to ambient pressure, as evidenced by the Rietveld refinement spectrum shown in Figure 1(e) for $Fe_{0.99}Ni_{0.01}Se_{0.5}Te_{0.5}$. Figure 2 shows refined powder x-ray diffraction pattern of NiAs –type hexagonal phase observed at 52 GPa. The solid line represents the calculated values using the Rietveld refinements of a hexagonal (*P6$_3$/mmc*) phase.

The evolution of lattice parameters of the tetragonal phase (a-axis and c-axis) with the application of pressure of $Fe_{0.99}Ni_{0.01}Se_{0.5}Te_{0.5}$ are shown in Figure.3 (a) and it reveals that large anisotropic compressibility exhibits up to 14 GPa. These results show a systematic moderate decreasing trend with the application of pressure is observed due to the existence of van der Waals interlayer gap between the $Fe_2(Se,Te)_2$ layers in the system. The decrease of c/a an axial

ratio in the tetragonal phase brings the tetrahedral layers closer to each other under pressure and it causes instability which leads to the structural change from tetragonal to NiAs- type hexagonal phase observed at 15 GPa as shown in Figure.3 (a). Further, the sudden change in the lattice parameters a- and c- were confirms structural transitions at 15 GPa. The fitting analysis shows considerable volume change (-6.8 % at 15 GPa) on transformation from tetragonal $P4/nmm$ to the NiAs-hexagonal ($P6_3/mmc$) phase and it is shown in Figure.3(b). The hexagonal phase is stable between 15 GPa to 52 GPa as evidenced from Fig.1(d) and Fig.3(b). A similar structural phase transition has been reported previously on $Fe(Se_{0.8}S_{0.2})$ and FeSe superconductors by other groups [3,32-35]. The unit cell volume drops around 15 % has been associated with the structural phase transition reported for the parent FeSe systems. Several structural studies indicate that pressure-induced tetragonal phase to β-FeSe phase at room temperature [3,4], which is similar to that of the $Fe_{0.99}Ni_{0.01}Se_{0.5}Te_{0.5}$ superconductors [4]. On the other hand, T_c enhanced much larger than the parent materials under pressure. However, $Fe_{1.03}Se_{0.57}Te_{0.43}$ system undergoes a discontinuous transformation of the low-temperature orthorhombic to the monoclinic phase above 3 GPa and it remains stable up to 14 GPa [20].

Magnetic Properties

The isothermal magnetization as a function of temperature *M(T)* measurements was carried out near T_c region with an applied magnetic field of 15 Oe in ZFC mode under pressure up to 1 GPa for single-crystalline $Fe_{0.99}Ni_{0.01}Se_{0.5}Te_{0.5}$ is shown in Figure.4. A sharp diamagnetic signal signals corresponding to superconducting transition temperature (T_c) is observed at ~ 8.6 K at ambient pressure and it is almost matches with the offset T_c of ~9 K obtained from electrical resistivity measurements for the same samples as shown in Figure.4. An application of pressure, T_c increases from 8.6 K to 14.7 K at ~ 1 GPa and found the positive pressure coefficient of ~

6.05 K/GPa and it is shown as inset of Figure.4. The observed positive pressure coefficient is higher than the pressure effect on $FeSe_{0.5}Te_{0.5}$ superconductor reported earlier [22,36]. The magnetic measurements under pressure above 1 GPa could not be measured due to the limitation in the pressure cell.

The isothermal magnetization M(H) studies under various fixed temperatures (3 K, 6 K, 9 K, 12 K, and 15 K) up to ~1 GPa for $Fe_{0.99}Ni_{0.01}Fe_{0.5}Te_{0.5}$ single crystal analysis is shown in Figure. 5 (a) and found to be a typical type-II superconductor. Figure.5 (b) shows the M-H curve at 3 K exhibits a wide-open loop up to the applied field of 0.5 Tesla. The lower critical field (H_{c1}) can be defined as the deviation from the linear M(H) curve is shown in the inset of Figure. 5 (b) and found to be H_{c1} ~130 Oe for $Fe_{0.99}Ni_{0.01}Fe_{0.5}Te_{0.5}$ superconductor which is less than the parent compound $FeSe_{0.5}Te_{0.5}$~ (~230 Oe) [37] and $Fe_{0.99}Co_{0.01}Se_{0.5}Te_{0.5}$ (~440 Oe) [38]. Further, it decreases from 130 Oe to 50 Oe on increasing the temperature from 2 to 9 K and H_{c1} is get suppressed nearer to T_c. Further, the width of the *M(H)* loops decreases with the increase of temperature suggest that the Fe magnetic moment is riding over the diamagnetic signal and the results exhibit some positive magnetic background near T_c^{onset}. However, the obtained results of *M(H)* curves at low-temperature are exhibit FM dome hysteresis which is due to the ordering of the Fe magnetic moments [39]. Above T_c, the samples exhibits in the ferromagnetic state, and these *M(H)* curves show a good approximation with above T_c of *M(T)* curve and its associate with the magnetic background of $Fe_{0.99}Ni_{0.01}Fe_{0.5}Te_{0.5}$ sample which coexists with the superconducting signal at lower temperatures T < Tc.

Transport properties

Figure.6 (a) shows the temperature dependence of the electrical resistivity [$\rho(T)$] of $Fe_{0.99}Ni_{0.01}Se_{0.5}Te_{0.5}$ under various applied pressures up to 20.6 GPa normalized to the resistivity

value at 200 K. The $\rho(T)$ under high pressures were measured using hybrid piston-cylinder hydrostatic pressure cell and a designer diamond anvil cell (D-DAC) up to 3 GPa and 3 - 20.6 GPa respectively. The in-situ pressure value in D- DAC is recorded during each $\rho(T)$ measurements at low-temperatures around T_c region using the Ruby fluorescence technique. The $\rho(T)$ at ambient pressure exhibits semi-metallic nature and the resistivity value increased slowly from 0.197 mΩ-cm (ρ_{300K}) to 0.223 mΩ-cm (ρ_{130K}-upturn). Further, reducing temperature resistivity reaches the maximum value ρ_{40K}=0.236 mΩ-cm and followed by a sudden drop to zero resistivity at T_c=9 K. Further, application of pressure, ρ_{300K} and ρ_{40K} values are decreased to 0.062 mΩ-cm, and 0.054 mΩ-cm respectively at 20.6 GPa, On the other hand, observed upturn in the low-temperature region (130K to T_c) shows semi-metallic nature at ambient pressure and becomes metallic and also upturn at low temperature is get completely suppressed at 1.5 GPa. Further, application of pressure up to 20.6 GPa, the normal state resistivity decreases, and enhancement of metallic nature is observed and it is due to the alignment of distorted structure and resulting in an increase of the number of charge carriers at the Fermi level of this system [40]. In general, there is a trend in the decrease of electrical resistivity with pressure that would imply the reduction of net electron–phonon scattering and it indicate that the densities of states (DOS) is reduced at the Fermi surface and leads to enhancement of metallic behaviour in $Fe_{0.99}Ni_{0.01}Fe_{0.5}Te_{0.5}$. Besides, T_c is determined as an intersection of two extrapolated lines drawn through 90% and 10% of the resistivity transition curve (as indicated in the figures. 6 (b). At ambient pressure, a sharp T_c is observed at ~ 9 K. By the application of pressure up to 3 GPa, the T_c increases from 9 K to 30.5K (dT_c/dP=+7.19 K/GPa) and then T_c slowly decreases to 19 K (dT_c/dP=-2.56 K/GPa) at 7.5 GPa is shown in Figure.6 (b). The positive pressure coefficient on T_c observed from both $\rho(T)$ and $M(T)$ measurements are found to be the same value up to 1 GPa

as shown in inset of Figure.4, and it is slightly higher than with earlier reported values on iron-based chalcogenide superconductors such as $FeSe_{0.5}Te_{0.5}$ (~ 5.8 K/GPa) and $FeSe_{0.5}Te_{0.5}$ (~ 4.1 K/GPa) reported by V.P.S. Awana *et al*., and S.I. Shylin *et al*., [22,35,41-42] which are compared with parent materials and listed in table.1. However, T_c reduces marginally above 3 GPa and some trend has been reported by others on similar materials [20,22]. The compression of the lattice under pressure is expected to deform the Fe-Se/Te tetrahedra and considerable changes on the critical parameters like the tetrahedral angle and anion height which has a subsequent effect on change in T_c [22]. The gradual decrease of T_c (>3 GPa) with a large transition width might be due to induced magnetic fluctuation by spin instability [9] and structural distortion under high pressure [42].

In this connection, the suppression of superconductivity is correlated with XRD measurements and its structural transition under high pressure. At 7.5 GPa, NiAs hexagonal phase peaks start appearing in additions to the tetragonal phase, on the other hand, T_c reaches at 19 K. Further application of pressure up to 10.9 GPa, superconductivity get vanished till 12 K of the measurable temperature range of the low-temperature systems and T_c decreases due to the appearance of mixed phase. Furthermore, the mixed TH-Phases completely transform into NiAs hexagonal phase at 15 GPa (Figure.1.c) and the value of electrical resistivity continues to decrease with the application of pressure up to 20.6 GPa. Therefore, we conclude that $Fe_{0.99}Ni_{0.01}Se_{0.5}Te_{0.5}$ sample becomes metallic and do not exhibit superconductivity behaviour until 12 K up to 20.6 GPa. The evolution of T_c from $\rho(T)$ under various pressures is more clearly shown in Figure. 6(b). Figure.7 shows the phase diagram of (T_c vs. pressure) of $Fe_{0.99}Ni_{0.01}Se_{0.5}Te_{0.5}$ superconductor measured from both $\rho(T)$ and $M(T)$ studies under pressures up to 20.6 GPa and correlate with high-pressure structural analysis up to 52 GPa. It reveals that

the T_c increases up to 3 GPa followed by decreasing trend up to 7.5 GPa, and then becomes non-superconducting in the measurable range down to 12 K of the measuring system. The *ρ(T)* measurements on present samples ($Fe_{0.99}Ni_{0.01}Se_{0.5}Te_{0.5}$) does not shows superconductivity above 14 GPa, however, undoped FeSe loses its superconducting signal around ~ 12 GPa [33]. Further, both cases, it's due to the occurrence of structural transition from tetragonal (*P4/nmm*) to hexagonal (*P6$_3$/mmc*) phase, which was completed above 15 GPa at room temperature as shown in Figure.7. The parent and doped FeSe shows phase diagram on a dome shaped and beyond the optimum doping or pressure leads to decrease of T_c and the similar dome-shaped behaviour exhibit in some other superconductors such as cuprates [43], Fe- based [44], BiS_2 based [45] and heavy fermion [46] superconductors. Further, the magnitude of resistivity decreases with the application of pressure suggests that hybridization between Fe and Se under pressure exhibits a strong electron correlation effect on $FeSe_{0.5}Te_{0.5}$ superconducting systems [42]. This argument, cannot exclusive explanation for the pressure dependence of T_c related with $h_{Se/Te}$ which might exceed the optimal value at higher pressure. Therefore, external pressure changes the lattice parameters favouring the superconducting T_c and its enhancement. The modification of band structure and Fermi surface under pressure which may play an important responsibility in iron pnictides and chalcogenides. However, the external pressure is affecting the charge carrier in the density of states and the topology of the Fermi surface. Hence, the charge transfer that appears from chalcogenide to the iron layer could also be induced by external pressure. Here, we conclude that the pressure effect on T_c of iron chalcogenides cannot be reduced by only one parameter ($h_{Se/Te}$) [30] and, further, its needed neutron diffraction studies for the better understanding of magnetic phase and it's a variation of T_c.

Conclusions

In Summary, we have demonstrated by a combined magnetic, transport, and structural study of $Fe_{0.99}Ni_{0.01}Fe_{0.5}Te_{0.5}$ which undergoes a pressure- induced transition from the tetragonal to NiAs –hexagonal phase at ~ 7.5 GPa. The *P6₃/mmc* phase becomes a major phase above 15 GPa. The high-pressure resistivity and magnetization studies of $Fe_{0.99}Ni_{0.01}Fe_{0.5}Te_{0.5}$ show that the external pressure sharply enhances the T_c from 9 to 30 K at the pressure rate of +7.19 K/GPa and it decreases with further increasing pressure above 3 GPa. We found a pressure-induced structural transformation from tetragonal to the NiAs-hexagonal phase where superconductivity is suppressed at 15 GPa in $Fe_{0.99}Ni_{0.01}Se_{0.5}Te_{0.5}$. Therefore, the additional parameters of electronic structure and a possible charge transfer under pressure are related to the corresponding change of T_c must be considered. And, the negative pressure coefficient on T_c above 3 GPa may be due to magnetic instability along with structural change at higher pressure. Our high-pressure results above 3 GPa indicate that the decrease in pressure coefficient that reduces the charge carriers at density of stats resulting in lowering the T_c and additional studies are required to understand the role of magnetic fluctuation studies using neutron diffraction studies under pressure.

Experimental Sections

The single crystalline of Ni-doped $Fe_{1-x}Ni_xSe_{0.5}Te_{0.5}$ (x=0.0, 0.01, 0.03, 0.05, 0.07, 0.10 and 0.20) was grown by a self-flux melt growth method. The detailed structural and morphological studies were carried out on well-characterized single crystals and it has been reported earlier by Maheshwari *et al.*, [14]. It is found that an increase of Fe concentration at site Ni leads to a monotonic decrease of T_c followed by suppression of superconductivity occurs in $FeSe_{0.5}Te_{0.5}$ superconductor. Here, we have chosen $Fe_{0.99}Ni_{0.01}Se_{0.5}Te_{0.5}$ sample for our detailed high pressure

and low-temperature investigations due to the highest T_c achieved in 1 % doped Ni-doped sample.

Materials Characterization

The temperature dependence of dc magnetization *M(T)* down to 2 K (Zero Field Cooling - ZFC method) and field-dependent magnetization *M(H)* measurements up to 0.5 T under various fixed temperatures were investigated under various applied pressures up to ~1 GPa (Easy Lab Technologies M cell) using Physical Property Measurement System – Variable Sample magnetometer (PPMS-VSM, Quantum Design, USA). The applied pressure was calculated by the pressure dependence of T_c on pure Sn (99.999%) as a pressure calibrant which was loaded into the capsule along with the sample. The Fluorinert FC #70 and FC #77 (1:1) was used as a pressure transmitting medium (PTM) in the piston-cylinder hydrostatic pressure cell up to 1 GPa. (i) The normalized electrical resistivity measurements under ambient and high pressures (up to 3 GPa) were carried out down to 4 K by the conventional four-probe method using clamp-type hybrid hydrostatic piston-cylinder pressure cell and Closed Cycle Refrigerator - Variable Temperature Insert (CCR-VTI) system (CIA, USA). The outer and inner cylinders are made of hardened Be (2%)-Cu and special steel alloy respectively. The applied pressure was calibrated using bismuth (Bi) phase transitions under pressure at room temperature and Daphene #7474 was used as a PTM [47] for this piston-cylinder pressure cell. The four electrical contacts were made with copper wire (0.15 mmϕ) and good quality silver paste. The single crystalline sample used for these experiments had nearly 1.2×0.7×0.4 mm^3 dimensions. The pressure was applied onto the piston-cylinder pressure cell through the 20- ton hydraulic press (Riken Kiki, Japan) at room temperature. (ii) The Φ300-μm culet sized eight-probe designer diamond anvils Cell (D-DAC) [48-50] were used to do electrical resistivity measurements under high pressure from 3 GPa to 21

GPa. The electrical contacts were made of the tungsten contact pads which were developed by lithographically deposited techniques onto the culet of the designer diamond anvil. A DAC loaded with solid steatite and its act as a pressure-transmitting medium to obtain the quasi hydrostatic pressure and also act as electrical insulation of the sample from the pre-indented metallic gasket. The gasket was made from a 200-μm-thick hardened MP35N foil preindented to 80-μm and a 120-μm diameter hole was drilled through the centre of the preindented region using an electric discharge machine (EDM). A thin crystallite (~ 80 × 20 × 40 μm^3) sample was placed on the centre of the culet to have good contact with the tungsten pads. The in-situ pressure was measured every time in D-DAC at low temperature by ruby fluorescence technique and it was calibrated by the ruby R1 and R2 emission lines. [51,52].

Structural analysis under pressure were studied using DAC which was composed of a two opposed diamond anvils with Φ300-μm culets and spring-steel gasket and it was preindented to a thickness of 40-μm, and a Φ50-μm hole was drilled in the centre of the indentation. The powdered $Fe_{0.99}Ni_{0.01}Se_{0.5}Te_{0.5}$ single crystals and fine Cu powders (3–6 μm, Alfa Aesar) were loaded into the sample space. The high pressure XRD measurements were carried out at the Advanced Photon Source, Argonne National Laboratory (APS- HPCAT) beam line 16-ID-B. The monochromatic x-rays utilized in the angle dispersive diffraction measurements [x-ray wavelength, λ = 0.40663 Å]. The copper lattice parameters obtained from the Rietveld refinement of the x-ray diffraction patterns of a mixed sample and copper powder [55]. The Birch- Murnaghan equation (1) was fitted to the equation of state data on both sample and copper [53-54] to determine the pressure exhibits on the sample.

$$P(V) = \frac{3B_0}{2}\left[\left(\frac{V_0}{V}\right)^{\frac{7}{3}} - \left(\frac{V_0}{V}\right)^{\frac{5}{3}}\right]\left\{1 + \frac{3}{4}\left(B_0' - 4\right)\left[\left(\frac{V_0}{V}\right)^{\frac{2}{3}} - 1\right]\right\} \text{---- (1)}$$

Where, B_0 is the bulk modulus, B_0' is the first derivative of bulk modulus and V_0 is the volume at ambient pressure. The fitted values for the pressure for copper are B_0= 121.6 GPa, B´ = 5.583, and V_0 = 11.802 $Å^3$/atom [53]. The recorded two-dimensional x-ray diffraction patterns were integrated using the Dioptas software [55]. The quantity of phase fraction is employed by Rietveld refinement using software GSAS-II [56].

Acknowledgments

We would like to acknowledge support from the U.S. National Science Foundation (NSF) under Grant No. DMR-1608682. Portions of this work were performed at HPCAT (Sector 16), Advanced Photon Source (APS), Argonne National Laboratory. HPCAT operations are supported by DOE-NNSA's Office of Experimental Sciences. The Advanced Photon Source is a U.S. Department of Energy (DOE) Office of Science User Facility operated for the DOE Office of Science by Argonne National Laboratory under Contract No. DE-AC02-06CH11357. M. Kannan and P.K. Maheshwari are thanks to CSIR for Senior Research Fellowship (SRF) and P.K.M thanks to AcSIR for pursuing Ph.D Degree. The author SA wishes to thank DST (SERB, ASEAN, PURSE, FIST), MHRD (RUSA, GIAN), UGC-DAE CSR (Indore), and BRNS (Mumbai) for financial support.

References

1. **T. Imai, K. Ahilan, F.L. Ning, T.M. McQueen, R.J. Cava:** Why Does Undoped FeSe Become a High-T_c Superconductor under Pressure?. *Phys. Rev. Lett.* **102,** 177005-177009 (2009).
2. **Y. Kamihara, T. Watanabe, M. Hirano, H. Hosono:** Iron-Based Layered Superconductor La[$O_{1-x}F_x$]FeAs (x = 0.05-0.12) with T_c = 26 K. *J. Am. Chem. Soc.* **130**, 3296-3296 **(**2008).

3. **S. Medvedev, T.M. McQueen, I. Trojan, T. Palasyuk, M. I. Eremets, R.J. Cava, S. Naghavi, F. Casper, V. Ksenofontov, G. Wortmann, C. Felser:** Electronic and magnetic phase diagram of β-$Fe_{1.01}Se$ with superconductivity at 36.7 K under pressure. *Nat. Mater.* **8**, 630-633 **(**2009**)**.
4. **S. Margadonna, Y. Takabayashi, Y. Ohishi, Y. Mizuguchi, Y. Takano, T. Kagayama, T. Nakagawa, M. Takata, K. Prassides:** Pressure evolution of the low-temperature crystal structure and bonding of the superconductor FeSe(T_c=37K). *Phys. Rev. B.* **80** 064506-064511 (2009).
5. **G. Garbarino, A. Sow, P. Lejay, A. Sulpice, P. Toulemonde, M. Mezouar, M. Nu´n˜ez-Regueiro**: High-temperature superconductivity (T_c onset at 34 K) in the high-pressure orthorhombic phase of FeSe, *Europhys. Lett.* **86,** 27001-27006 (2009).
6. **C. Wang, S. Jiang, Q. Tao, Z. Ren, Y.K. Li, L.J. Li, C. Feng, J.H. Dai, G.H. Cao:** Superconductivity in $LaFeAs_{1-x}P_xO$: Effect of chemical pressures and bond covalency. *Europhys. Lett.* **82,** 47002-47007 (2009).
7. **W. Guan,Y.H. Xu, S.R. Sheen, Y.C. Chen, Y.J.T. Wei, H.F. Lai, M.K. Wu, J.C. Ho:** Ion-size effect on TN in (R, Pr„)$Ba_2Cu_30_7$ systems (R =Lu, Yb, Tm, Er, Y, Ho, Dy, Gd, Eu, Sm, and Nd). *Phys. Rev. B.* **49**, 15993-15999 (1994).
8. **E. Böhmer, V. Taufour, W. E. Straszheim, T. Wolf, P.C. Canfield**, Variation of transition temperatures and residual resistivity ratio in vapor-grown FeSe, *Phys. Rev. B*, **9**, 024526-024531 (2016).
9. **F. Hardy, M. He, L. Wang, T. Wolf, P. Schweiss, M. Merz, M. Barth, P. Adelmann, R. Eder, A.A. Haghighirad C. Meingas:** Calorimetric evidence of nodal gaps in the nematic superconductor FeSe. *Phys. Rev. B*, **99,** 035157-035168 (2019).

10. **M.H. Fang, H.M. Pham, B. Qian, T.J. Liu, E.K. Vehstedt, Y. Liu, L. Spinu, Z.Q. Mao:** Superconductivity close to magnetic instability in $Fe(Se_{1-x}Te_x)_{0.82}$. *Phys. Rev. B,* **78**, 224503-224507 (2008).
11. **Y. Mizuguchi, F. Tomioka, S. Tsuda, T. Yamaguchi, Y. Takano**: Superconductivity in S-substituted FeTe. *Appl. Phys. Lett*, **94,** 012503-012505 (2009).
12. **Y. Mizuguchi, F. Tomoiioka, S.Tsuda, T. Yamaguchi, Y. Takano:** Substitution Effects on FeSe Superconductor. J. Phys. Soc Jpn. **78**, 074712-074716 (2009).
13. **R. Shipra, H. Takeya, K. Hirata, A. Sundaresa**: Effects of Ni and Co doping on the physical properties of tetragonal $FeSe_{0.5}Te_{0.5}$ superconductor. *Physica C*. **470**, 528-532 (2010).
14. **P.K. Maheshwari, B. Gahtori, V.P.S. Awana:** Fast suppression of superconductivity with Fe site Ni doping in $Fe_{1-x}Ni_xSe_{0.5}Te_{0.5}$ single crystals (x = 0.0 to 0.20). J. *Sup. & Novel Mag*, **29**, 2473-2478 (2016).
15. **L. Sang, B. Shabbir, P.K. Maheshwari, W. Qiu, Z. Ma, S. Dou, C. Cai, V.P.S. Awana, X. Wang:** Hydrostatic pressure-induced huge enhancement of critical current density and flux pinning in $Fe_{1-x}Co_xSe_{0.5}Te_{0.5}$ single crystals. *Supercond. Sci. Technol.* **31**, 025009-025016 (2018).
16. **M. K. Wu, F.C. Hsu, K.W. Yeh, T.W. Huang, J.Y. Luo, M.J. Wang, H.H. Chang, T.K. Chen, S.M. Rao, B.H. Mok, C.L. Chen, Y.L. Huang, C.T. Ke, P.M. Wu, A.M. Chang, C.T. Wu, T.P. Perng**: The development of the superconducting PbO-type β-FeSe and related compounds. *Physics C.* **469,** 340-349 (2009).
17. **Kumar, R.P. Tandon, V.P.S. Awana:** Effect of 3d metal (Co and Ni) doping on the superconductivity of $FeSe_{0.5}Te_{0.5}$. *IEEE trans. Mag.* **48,** 4239-4242 (2012).

18. **K.W. Yeh, T.W. Huang, Y. Huang, T.K. Chen, F.C. Hsu, P.M. Wu, Y.C. Lee, Y.Y. Chu, C.L. Chen, Y.J. Luo, D.C. Yan, M.K. Wu:** Tellurium substitution effect on superconductivity of the α-phase iron selenide. *Euro phys. Lett*,.**84**, 37002-37005 (2008).
19. **K. Horigane, H. Hiraka, K. Ohoyama**: Relationship between Structure and Superconductivity in $FeSe_{1-x}Te_x$. *J. Phys. Soc. Japan.* **78**, 074718-074722 (2009).
20. **N.C. Gresty, Y. Takabayashi, A.Y. Ganin, M.T. McDonald, J.B. Claridge, D. Giap, Y. Mizuguchi, Y. Takano, T. Kagayama, Y. Ohishi, M. Takata, M.J. Rosseinsky, S. Margadonna, K. Prassides**: Structural phase transitions and superconductivity in $Fe_{(1+delta)}Se_{0.57}Te_{0.43}$ at ambient and elevated pressures. *J. Am. Chem. Soc.***131**, 16944-16952 (2009).
21. **S. Karmakar:** Measurement of improved pressure dependence of superconducting transition temperature. *High Pressure Res.* **33,** 381-391 (2013).
22. **G. Tsoi, A.K. Stemshorn, Y.K. Vohra, P.M. Wu, F.C. Hsu, Y.L. Huang, M.K. Wu, K.W. Yeh, S.T. Weir:** High pressure superconductivity in iron-based layered compounds studied using designer diamonds. *J. Phys.: Condens. Matter.* **21,** 232201-232204 **(**2009**)**.
23. **M. Gooch, B. Lorenz, S.X. Huang, C.L. Chien and C.W. Chu**: Pressure effects on strained $FeSe_{0.5}Te_{0.5}$ thin films. *J. Appl. Phys.* **111**, 112610-112614 (2012).
24. **A.K. Stemshorn, Y.K. Vohra, P.M. Wu, F.C. Hsu, Y.L. Huang, M.K. Wu, K.W. Yeh:** Pressure-induced reversible amorphization in superconducting compound $FeSe_{0.5}Te_{0.5.}$ *High Pressure Res.* **29,** 267-271 **(**2009**)**.
25. **J. Kumar, S. Auluck, P.K. Ahluwalia, V.P.S. Awana**: Chalcogen height dependence of magnetism and Fermiology in $FeTe_xSe_{1-x}$. *Supercond Sci. Technol.* **25**, 095002-095011 (2012).

26. **C.Y. Moon, H.J. Choi:** Chalcogen-Height Dependent Magnetic Interactions and Magnetic Order Switching in $FeSe_xTe_{1-x}$. *Phys. Rev. Lett.* **104**, 057003-057012 (2010).

27. **Ciechan, M. Winiarski, M.S. Czeka:** The Pressure Effects on Electronic Structure of Iron Chalcogenide Superconductors $FeSe_{(1-x)}Te_{(x)}$. *Acta Phys. Pol. A.* **121**, 820-823 (2012).

28. **T. McQueen, A. Williams, P. Stephens, J. Tao, Y. Zhu, V. Ksenofontov, F. Casper, C. Felser, R. Cava:** Tetragonal-to-Orthorhombic Structural Phase Transition at 90 K in the Superconductor $Fe_{1.01}Se$. *Phys. Rev. Lett.* **103**, 57002-57005 (2009).

29. S**.H. Baek, D.V. Efremov, J.M. Ok, J.S. Kim, J.D. Brink, B. B¨uchner:** Orbital-driven nematicity in FeSe. *Nat. Mater*. **14**, 210-214 (2015).

30. **H. Okabe, N. Takeshita, K. Horigane, T. Muranaka, J. Akimitsu:** Pressure-induced high-T_c superconducting phase in FeSe: Correlation between anion height and T_c. *Phys. Rev. B.* **81**, 205119-205124 (2010).

31. **K. Stemshorn, G. Tsoi, Y.K. Vohra, S. Sinogeiken, P.M. Wu, Y. Huang, S.M. Rao, M.K. Wu, K.W. Yeh, S.T. Weir:** Low temperature amorphization and superconductivity in FeSe single crystals at high pressures**,** *J. Mater. Res*, **25**, 396-402 (2010).

32. **H. Takahashi, T. Tomita, H. Takahashi, Y. Mizuguchi, Y. Takano, S. Nakano, K. Matsubayashi, Y. Uwatoko:** High-pressure studies on T_c and crystal structure of iron chalcogenide superconductors. *Sci. Technol. Adv. Mater.* **13**, 054401-054407 (2012).

33. **R.S. Kumar, Y. Zhang, S. Sinogeikin, Y. Xiao, S. Kumar, P. Chow, L.A. Cornelius:** Crystal and Electronic Structure of FeSe at High Pressure and Low Temperature. *J. Phys. Chem. B.* **114,** 12597-12606 (2010).

34. **D. Braithwaite, B. Salce, G. Lapertot, F. Bourdarot, C. Marin, D. Aoki, M.J. Hanfland:** Superconducting and normal phases of FeSe single crystals at high pressure. *J. Phys.: Condens. Matter.* **21,** 232202-232206 **(**2009**)**.

35. **S. I. Shylin, V. Ksenofontov, P.G. Naumov, S.A. Medvedev, V. Tsurkan, J. Deisenhofer, A. Loidl, L.M. Schoop, T. Palasyuk, G. Wortmann, C. Felser:** Pressure effect on superconductivity in $FeSe_{0.5}Te_{0.5}$. *Phys. Status Solidi B.* **254,** 1600161-1600167 (2017).

36. **K. Horigane, N. Takeshita, C.H. Lee, H. Hiraka, K. Yamada:** First Investigation of Pressure Effects on Transition from Superconductive to Metallic Phase in $FeSe_{0.5}Te_{0.5}$. *J. Phys. Soc. Jpn.* **78,** 063705-063707 (2009).

37. **A.B. Karki, V.O. Garlea, R. Custelcean, S. Stadler, E.W. Plummer, R. Jina**, Interplay between superconductivity and magnetism in $Fe_{(1-x)}Pd_{(x)}Te$. *Proc Natl Acad Sci (U S A).* **110**, 9283-9288 (2013).

38. **P.K. Maheshwari, B. Gahtori, A. Gupta, V.P.S. Awana:** Impact of Fe site Co substitution on superconductivity of $Fe_{1-x}Co_xSe_{0.5}Te_{0.5}$ (x = 0.0 to 0.10): A flux free single crystal study. *AIP Advances.* **7**, 015006 -015016 (2017).

39. **P.K. Maheshwari, R. Jha, B. Gahtori, V.P.S. Awana:** Flux Free growth of large $FeSe_{0.5}Te_{0.5}$ superconducting single crystals by an easy high temperature melt and slow cooling method. *AIP Advances*. **5,** 097112-097122 (2015).

40. **S. Thrupathiah, J. Fink, P.K. Maheshwari, V.V. Ravikishore, Z.H. Liu, E.D.L. Rienks, V.P.S. Awana, D.D. Sarma:** The effect of impurity substitutions on the band structure and the electronic correlation of the strongly correlated $FeSe_{0.5}Te_{0.5}$ superconductor. *Phys. Rev. B.* **93,** 205143-205149 **(**2016**)**.

41. **C.L. Huang, C.C. Chou, K.F. Tseng, Y.L. Huang, F.C. Hsu, K.W. Yeh, M.K. Wu, H. Yang:** Pressure effects on superconductivity and magnetism in $FeSe_{1-x}Te_x$. *J. Phys. Soc. Japan.* **78,** 084710-084713 **(**2009**)**.
42. **R. Jha, Rayees, A. Zargar, A. Hafiz, H. Kishan, V.P.S. Awana:** Superconductivity at 25K under hydrostatic pressure for $FeTe_{0.5}Se_{0.5}$ superconductor. *J. Sup. Novel Mag.* **27,** 897 -901 (2014).
43. **P.A. Lee, N. Nagaosa, X.G. Wen:** Doping a Mott insulator: Physics of high-temperature superconductivity. *Rev. Mod. Phys.* **78,** 17-85 (2006).
44. **H. Takahashi, K. Igawa, K. Arii, Y. Kamihara, M. Hirano, H. Hosono:** Superconductivity at 43 K in an iron-based layered compound $LaO_{(1-x)}F_{(x)}FeAs$. *Nature.* **453,** 376-378 (2008).
45. **G. Kalai Selvan, G. Thakur, K. Manikandan, A. Banerjee, Z. Haque, L.C. Gupta, A.K. Ganguli, S. Arumugam:** Superconductivity in $La_{1-x}Sm_xO_{0.5}F_{0.5}BiS_2$ ($x= 0.2,\ 0.8$) under hydrostatic pressure. *J. Phys. D: App. Phys.* **49**, 275002-275008 (2016).
46. **V.A. Sidorov, M. Nicklas, P.G. Pagliuso, J.L Sarrao, Y. Bang, A.V. Balatsky, J.D. Thompson:** Superconductivity and quantum criticality in $CeCoIn_5$. *Phys. Rev. Lett.* **89**, 157004-157007 (2002).
47. **N. Mori, H. Takahashi, N. Takeshita:** Low-temperature and high-pressure apparatus developed at ISSP, University of Tokyo. *High Press. Res*, **24,** 225-232 (2004).
48. **S.T. Weir, J. Akella, C.A. Ruddle, Y.K. Vohra, S.A. Catledge:** Epitaxial diamond encapsulation of metal microprobes for high pressure experiments. *Appl. Phys. Lett.* **77**, 3400-3402 (2000).

49. **J.R. Patterson, S.A. Catledge, Y.K. Vohra, J. Akella, S. T. Weir:** Electrical and mechanical properties of C_{70} fullerene and graphite under high pressures studied using designer diamond anvils. *Phys. Rev. Lett.* **85,** 5364-5367 **(**2000**)**.

50. **D.D. Jackson, J.R. Jeffries, W. Qiu, G.D. Griffith, S. McCall, C. Aracne, M. Fluss, M.B. Maple, S.T. Weir, Y.K. Vohra**: Structure-dependent ferromagnetism in Au_4V studied under high pressure. *Phys. Rev. B.* **74**, 174401-174408 (2006).

51. **H.K. Mao, J. Xu, P.M. Bell:** Calibration of the ruby pressure gauge to 800 kbar under quasi-hydrostatic conditions. *J. Geophys. Res.* **91,** 4673-4678 (1986).

52. **W. L. Vos, J. A. Schouten:** On the temperature correction to the ruby pressure scale. *J. Appl. Phys*. **69,** 6744-6749 (1991).

53. **N. Velisavljevic, Y.K. Vohra:** Distortion of Alpha-Uranium Structure in Praseodymium Metal to 311 GPa. *High Pressure Res.* **24**, 295-302 (2004).

54. **F. Birch**: Finite Elastic Strain of Cubic Crystals. *Phys. Rev.* **71,** 809-825(1947).

55. **C. Prescher, V.B. Prakapenka:** DIOPTAS: a program for reduction of two-dimensional X-ray diffraction data and data exploration. *High Pressure Res.* **35**, 223-230 (2015).

56. **B.H. Toby, R.B.V. Dreele:** GSAS-II: the genesis of a modern open-source all purpose crystallography software package. *J. Appl. Crystallogr*. **46**, 544-549 (2013).

Figure Captions:

Figure 1: (color online) The integrated x-ray diffraction pattern for tetragonal and NiAs hexagonal phases of $Fe_{0.99}Ni_{0.01}Se_{0.5}Te_{0.5}$ recorded at various pressures with monochromatic radiation of wavelength λ=0.4066 Å. (**a**), The powder XRD pattern shows tetragonal (*P_4/nmm*) phase at 0.5 GPa, (**b**) Coexistence of tetragonal and shows NiAs hexagonal phase at 7.5 GPa, (**c, d**) NiAs-hexagonal (*$P6_3/mmc$*) phases at 15 GPa and 52 GPa respectively (**e**) Tetragonal phase at 0.1 MPa (decompression). The peaks marked with an asterisk are from the copper as a pressure standard.

Figure 2: (color online) Rietveld crystal structure refinement of the $Fe_{0.99}Ni_{0.01}Se_{0.5}Te_{0.5}$ superconductor at the 52 GPa. The solid line represents the calculated values using the Rietveld refinements assuming as a tetragonal (*$P6_3/mmc$*) phase.

Figure 3: (color online) (a) The measured lattice parameters a-axis (black), c-axis (blue) as a function of pressure up to 52 GPa and (b) The volume changes (V/Vo) as a function of pressure up to 52 GPa at room temperature for $Fe_{0.99}Ni_{0.01}Se_{0.5}Te_{0.5}$. The solid circle curve is a Birch-Murnaghan fit to the data untill 52 GPa and include tetragonal (*P_4/nmm*) and NiAs-hexagonal (*$P6_3/mmc$*) phases.

Figure 4: (color online) The dc magnetization recorded at 15 Oe as a function of temperature at various applied pressures up to ~ 1 GPa for single-crystalline $Fe_{0.99}Ni_{0.01}Se_{0.5}Te_{0.5}$ and shows the methodology of T_c marking at ~ 1 GPa. Inserts show T_c vs P phase diagram.

Figure 5: (color online) (a) Magnetic hysteresis loops for $Fe_{0.99}Ni_{0.01}Se_{0.5}Te_{0.5}$ as a function of the applied field (H) up to 5 kOe at selected temperatures of 3,6,9,12 and 15 K at ~ 1 GPa (**b**) The bulk superconducting hysteresis loop observed at 3 K and arrow marks indicate the methodology of observed lower critical field (H_{c1}) (Insets).

Figure 6: (color online) (a) Normalized resistivity of ρ(T)/ρ(200K) under various applied hydrostatic pressures from 0 to ~21 GPa, (b) shows an enlarged view of *ρ(T)* in the low-temperature superconducting region (4- 50 K) for $Fe_{0.99}Ni_{0.01}Se_{0.5}Te_{0.5}$ superconductors.

Figure 7: Experimental phase diagram of a variation of T_c under pressure obtained from resistivity (purple) and magnetic (yellow) measurements correlate with structural analysis for $Fe_{0.99}Ni_{0.01}Se_{0.5}Te_{0.5}$ superconductors.

Table I: Correlation with pressure dependence of T_c with various chalcogenide superconductors.

Sample	Ambient Tc	Pressure maximum (Tc)	dTc/dP	Reference
FeSe	8 K	27 K (1.5 GPa)	9.1 K/GPa	Y. Mizuguchi et al., Appl. Phys. Letters 94, 152505 (2008).
FeSe- Single crystal	9 K	28 (2.43 GPa)	8 K/GPa	Soon-Gil Jung et al., Scientific Reports 5, 16385 (2015)
$Fe_{0.99}Ni_{0.01}Se_{0.5}Te_{0.5}$	9 K	30.5 (3 GPa)	7.19 K/GPa	Kalaiselvan et al.,(Present Results)
FeSe	7.5 K	34 K (7 GPa)	3.7 K/GPa	Kiyotaka Miyoshi et al., J. Phys. Soc. Jpn. 83, 013702 (2014)
FeSe	8 K	36 K (9.5 GPa)	2.9 K/GPa	Andrew K. Stemshorn et al J. Mater. Res., 25, 2 (2010)
$FeSe_{0.5}T_{0.5}$	13.5	26.2 (2 GPa)	6.35 K/GPa	K. Horigane et al., J. Phys. Soc. Jpn. 78, 063705 (2009)
$Fe_{1.03}Se_{0.57}Te_{0.43}$	13.9 K	26.3 (2.3 GPa)	6.2 K/GPa	N. C. Gresty et al., J. Am. Chem.Soc. 131, 16944 (2009)
$LaFeAsO_{0.89}F_{0.11}$	28 K	43 K (3 GPa)	8 K/GPa	H. Takahashi et al., Nature 453, 376 (2008)

Figure 1.

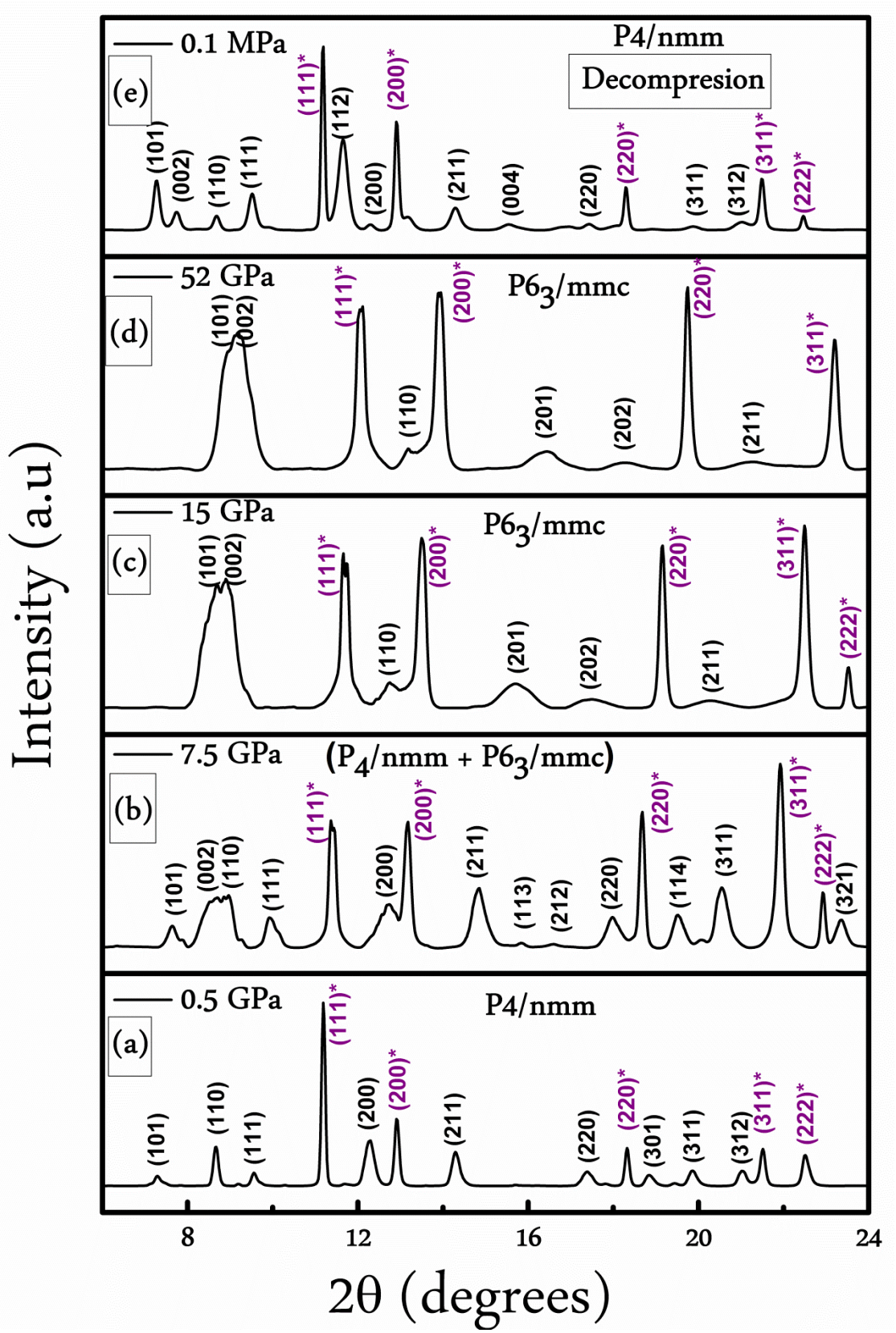
0.1 MPa
(e)
P4/nmm
Decompresion
(101)
(002)
(110)
(111)
(111)*
(112)
(200)
(200)*
(211)
(004)
(220)
(220)*
(311)
(312)
(311)*
(222)*
52 GPa
(d)
P6$_3$/mmc
(101)
(002)
(111)*
(110)
(200)*
(201)
(202)
(220)*
(211)
(311)*
15 GPa
(c)
P6$_3$/mmc
(101)
(002)
(111)*
(110)
(200)*
(201)
(202)
(220)*
(211)
(311)*
(222)*
7.5 GPa
(P$_4$/nmm + P6$_3$/mmc)
(b)
(101)
(002)
(110)
(111)
(111)*
(200)
(200)*
(211)
(113)
(212)
(220)
(220)*
(114)
(311)
(311)*
(222)*
(321)
0.5 GPa
P4/nmm
(a)
(101)
(110)
(111)
(111)*
(200)
(200)*
(211)
(220)
(220)*
(301)
(311)
(312)
(311)*
(222)*
Intensity (a.u)
8
12
16
20
24
2θ (degrees)

Figure 2.

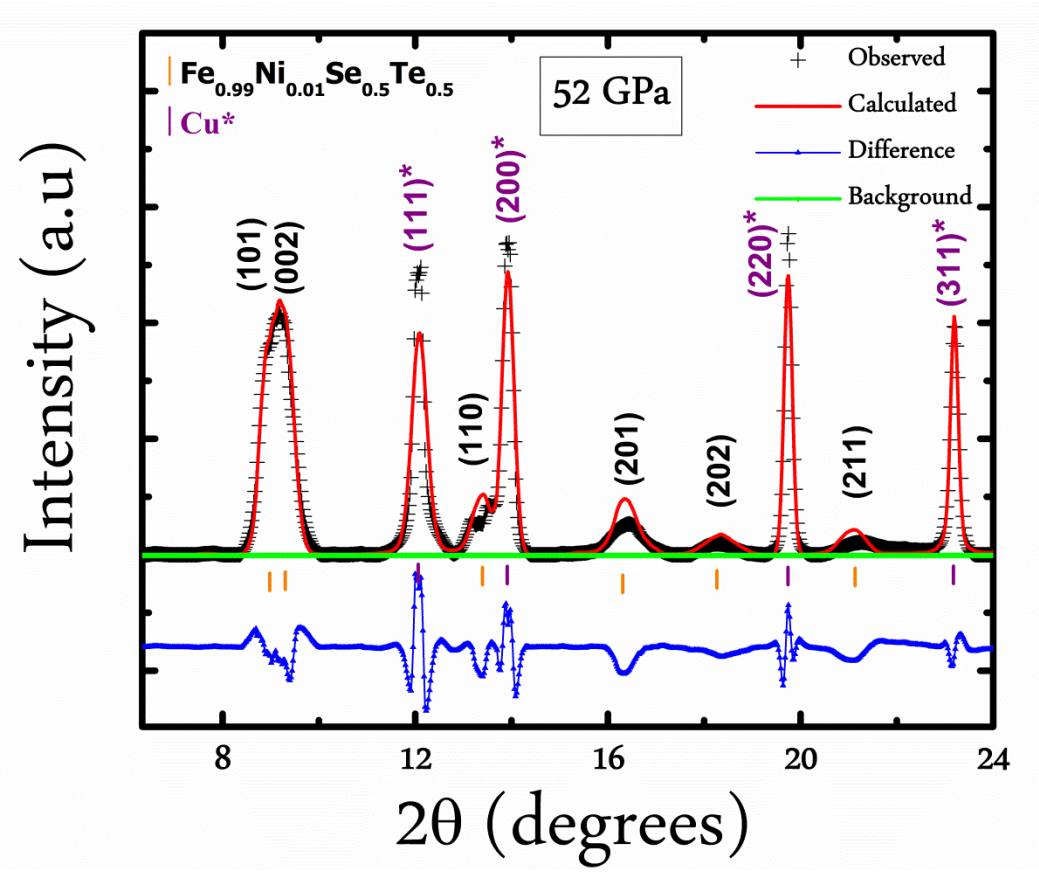
Fe0.99Ni0.01Se0.5Te0.5
Cu*
52 GPa
Observed
Calculated
Difference
Background
(101)
(002)
(111)*
(110)
(200)*
(201)
(202)
(220)*
(211)
(311)*
Intensity (a.u)
8
12
16
20
24
2θ (degrees)

Figure 3.

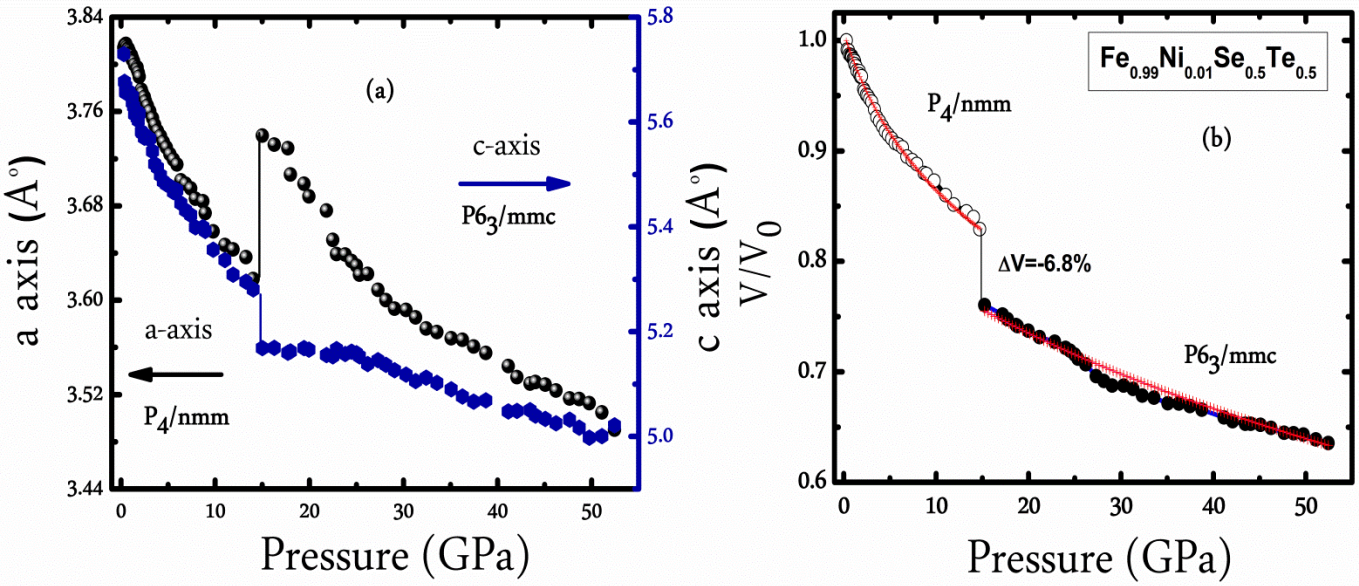

Figure 4.

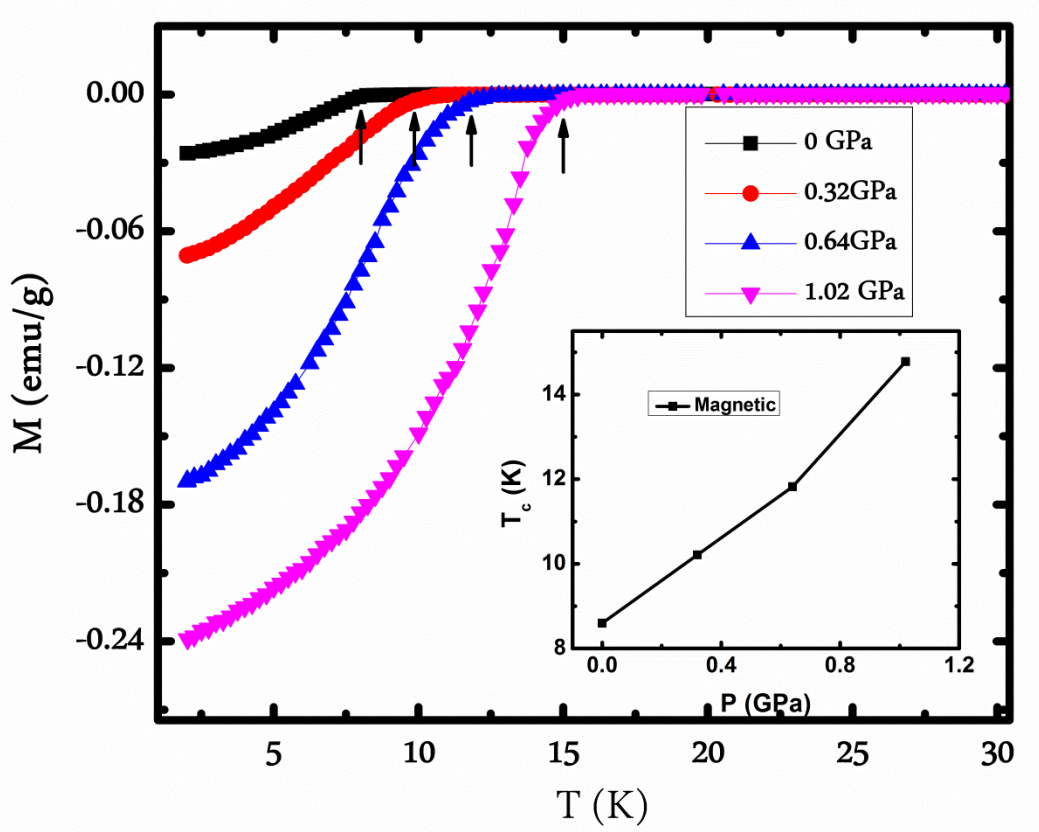

Figure 5.

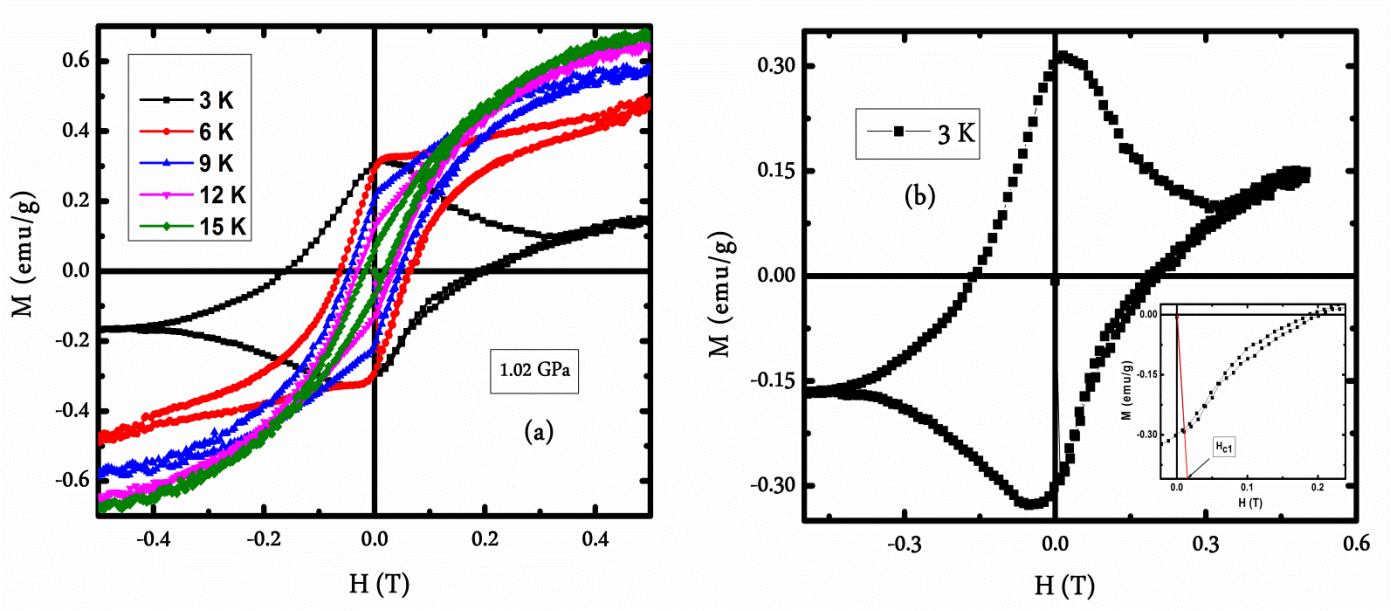

Figure 6.

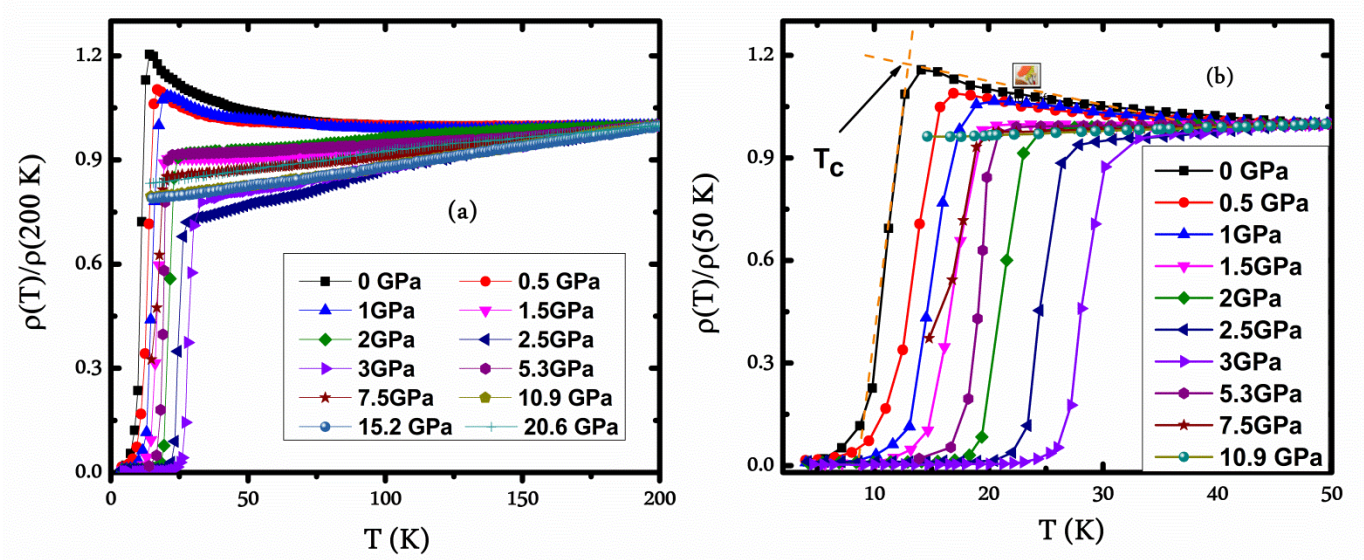

Figure 7.

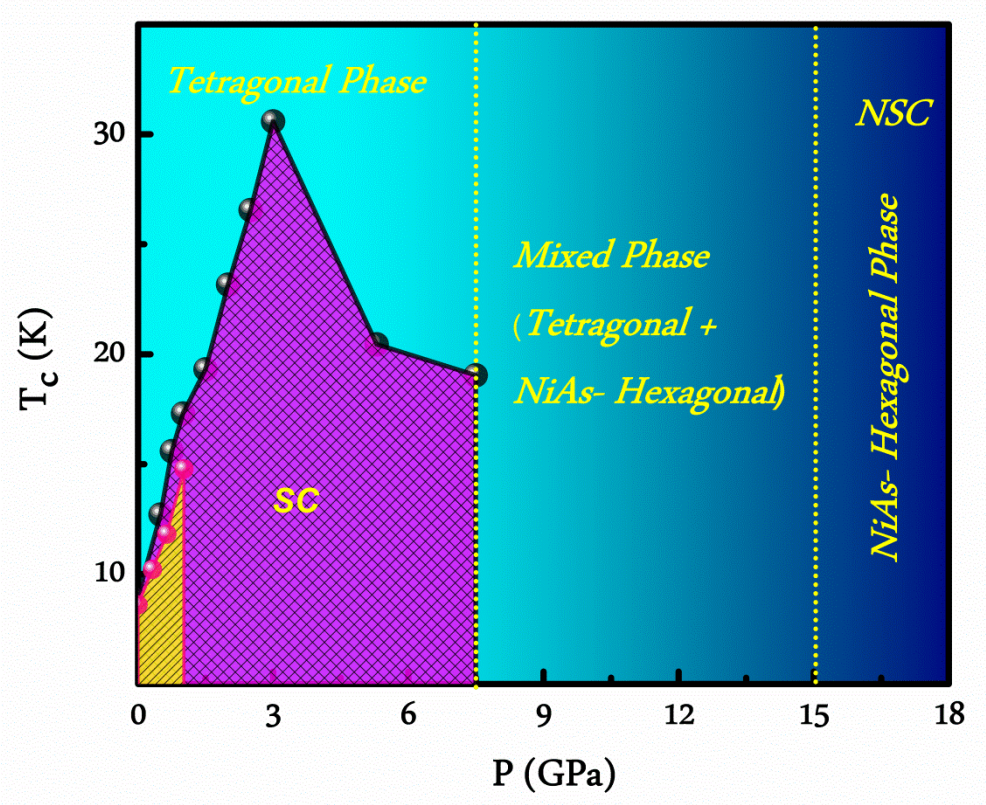
Tetragonal Phase
Mixed Phase
(Tetragonal +
NiAs- Hexagonal)
NSC
NiAs- Hexagonal Phase
SC
T_c (K)
30
20
10
0
3
6
9
12
15
18
P (GPa)